NANOSTRUCTURED MATERIALS FOR PHOTOELECTROCHEMICAL WATER SPLITTING APPLICATION

MOHIT

DEPARTMENT OF PHYSICS

INDIAN INSTITUTE OF TECHNOLOGY DELHI

JULY 2023

NANOSTRUCTURED MATERIALS FOR PHOTOELECTROCHEMICAL WATER SPLITTING APPLICATION

by

MOHIT

Department of Physics

Submitted

in fulfilment of the requirements of the degree of Doctor of Philosophy

to the

INDIAN INSTITUTE OF TECHNOLOGY DELHI

JULY 2023

Dedication

I want to dedicate this thesis work

to the Supreme Almighty God, Parents,

Grandparents, and Teachers

Certificate

This is to certify that, the thesis entitled **"Nanostructured materials for photoelectrochemical water splitting application"** being submitted by **Mohit** to the Department of Physics, **Indian Institute of Technology Delhi** is worthy of consideration for the award of the degree of Doctor of Philosophy and is a record of the original bonafide research work carried out by him under my guidance and supervision. The results contained in it have not been submitted in part or full to any other university or institute for the award of any degree or diploma.

NChare
24/7/23

Prof. Neeraj Khare
Department of Physics
Indian Institute of Technology Delhi
Hauz Khas, New Delhi-110016,
India.

Acknowledgements

First of all, I am thankful to "Almighty God" for my existence and blessings. I always feel his kind presence in life in various ways which give me positive energy to think and work progressively. It has been a great privilege for getting the opportunity to express my indebtedness and sincere thanks to my respected supervisor, Prof. Neeraj Khare, as his invaluable guidance, motivation, and expertise made this work possible. I appreciate his politeness and continuous encouragement in carrying out the research work successfully. His important lessons will always remain with me in life. It gives me immense pleasure to express my sense of gratitude to Dr. Sangeeta Khare for sharing her experiences and knowledge.

I would like to express my thankfulness to my SRC members, Prof. Santanu Ghosh, Prof. Rajendra Singh, and Prof. Sandeep Kumar Jha for evaluating my progress in each stage of my research work and giving their valuable suggestions for improvement. My sincere thanks to Prof. Pankaj Srivastava, Head of the Physics Department, IIT Delhi for providing various research facilities. I am thankful to Prof. Sujeet Chaudhary, DRC chairperson, Physics Department IIT Delhi for giving his time and support in overviewing the progress of the research work. I extend my thanks to Nanoscale Research Facility (NRF), Central Research Facility (CRF), and other technical staff of IIT Delhi for providing characterization facilities and technical assistance during the period of my research work.

My sincere thanks to my fellow lab mates of Nano Functional Oxide Superconductivity Laboratory (NFOSL), Dr. Mohd. Zubair Ansari, Dr. Deepti Chaudhary, Dr. Simrjit Singh, Dr. Deepanshu Sharma, Dr. Sandeep Munjal, Dr. Mohd. Faraz, Dr. Surbhi Sharma, Dr. Satyendra Prakash Pal, Dr. Rohit Kumar, Dr. Kannan U. M, Dr. Sunil Kumar, Dr. Pratisha Gangwar, Dr. Huidrom Hemojit Singh, Dr. Mamta Dahiya, Dr. Dheeraj Kumar, Dr. Nitish Kumar, Dr. Gaurav Sharma, Dr. Birendra, Mrs. Abhilasha Chouksey, Mr. Amish Kumar Gautam, Mr. Gaurav Kumar, Mr. Arun Mondal, Mr. Aman Sharma, Mr. Manoj Singh, Ms. Rajni, Mr. Sandeep Goyal, and Ms. Sarita Mittal for helping in various ways and maintaining a healthy atmosphere to work in the lab. I especially thank Dr. Dheeraj Kumar, Dr. Mohd. Faraz, and Dr. Mamta Dahiya for sharing their experiences and knowledge. I enjoyed the discussions while having evening tea or coffee with our supervisor and lab mates; pizza and burger parties on special occasions and outings worked as a stress buster and refreshed my mind. I have learnt many things from every lab mate. I wish them good luck and success in their future endeavors.

I would like to offer my prayers to my beloved grandparents, Late. Shri. Mohar Singh, Late. Smt. Sarwati Devi on this most memorable day of my life. I especially express my profound gratitude to my grandparents for their blessing which gave me hope and strength in life. Most importantly, I wish to thank my loving parents Mr. Suresh Kumar and Mrs. Urmila Devi who have always supported and encouraged me to do my best in all matters of life. I put my deepest sense of regard and gratefulness to my elder sisters, Mrs. Manisha, and Mrs. Madhu Bala for their incredible love, emotional and mental support throughout my life. They truly understood my problems during various phases of life and provided family support whenever I needed it the most. I am fortunate to thank all times and believing in me, standing with me in my good and bad times, and providing their endless support in the personal and professional forefront.

I would like to special thanks to my teacher, Dr. Rishi Vyas, Dr. K.C. Bhamu, Dr. Pankaj Goswami, and Dr. Preetam Singh Gaur for inspiring and motivating me for creating interest to go for higher studies.

I also thank my friends Mr. Raj Kumar, Mr. Vishnu Dutt Kaushik, Mr. Tinku Yadav, Ms. Mohini Manav, Ms. Nidhi Dalal, Mrs. Manjeeta, Ms. Gurmeet Kaur, Mrs. Sundarpreet Kaur, Ms. Gauri Rajput, Ms. Divya Rajput, Mr. Puru Rajput, Ms. Pooja Rajput, Mr. Aashish More, Mr. Devendra Kumar, Mr. Manjeet, Mr. Pritam, Mr. Manoj Kumar, Mr. Nitesh Kumar, Mr. Jitendra Arya, Mr. Anil Kumar, Mr. Rakesh Gangwar, Mr. Rishikesh Kushwaha, Mr. Himanshu Arora, Mr. Saurabh Pandey, Mr. Jamal Ahmed Khan, Ms. Pariksha Malik, Ms. Rekha Aggarwal, Mr. Ram Singh, Mr. Himanshu Bangar, Mr. Amar Kumar, Ms. Pratiksha Chaudhary, Ms. Preeti Bhumla, Ms. Shobha Singh, Ms. Ekta Yadav, Mr. Shiv Luv Chauhan, Mr. Govind Prasad, Mr. Kamlesh, Mr. Amit Gupta, Mr. Pradeep for being so friendly and supportive. I am grateful to have badminton teammates like Mr. Arjun Kumar, Mr. Dhananjay Verma, and Mr. Vaibhav Sharma, who have not only contributed to my physical fitness but have also helped me to develop an interest in sport. I am tempted to individually thank all my friends and well-wishers who, from my childhood until now, have helped me in various ways.

Finally, I gratefully acknowledge the financial assistance which I received from the Ministry of Electronics and Information Technology (MeitY), Department of Science and Technology (DST), India, Junior Research Fellowship (JRF) and Senior Research Fellowship (SRF) from CSIR during my Ph.D. work.

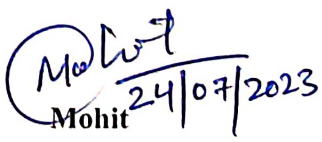

Mohit

Abstract

Continuous power consumption has been driving the economy since the onset of the industrial and urban revolutions. However, the burning of fossil fuels to meet this demand has resulted in global warming and a host of health problems, making the search for a sustainable and eco-friendly energy source a pressing issue for future generations. The combustion-based energy conversion process is particularly problematic and calls for the development of a carbon-free and renewable energy source that can benefit society without harming the environment. Hydrogen fuel is a promising alternative that can meet these requirements. A significant approach to generating sustainable energy is photoelectrochemical water splitting, which can produce hydrogen and oxygen. This study focuses on the synthesis of semiconductor nanostructures and nanocomposites and explores its application for photoelectrochemical water splitting to generate hydrogen.

To work in this direction, synthesis of cubic and hexagonal phase of visible light active $ZnIn_2S_4$ (ZIS) by hydrothermal method using two different precursors to explore its potential for use in PEC water splitting. The selection of precursors plays a crucial role in controlling the phase of the material. The structural, morphological, and optical properties of $ZnIn_2S_4$ (ZIS) were analyzed using various characterization techniques. Additionally, the photoelectrochemical properties of the fabricated ZIS photoelectrode were examined. Cubic-ZIS (C-ZIS) photoelectrode achieved a current density of ~80 $\mu A/cm^2$ at 0.8 V vs. Ag/AgCl, while the hexagonal ZIS (H-ZIS) achieved a current density of ~60 $\mu A/cm^2$ at 0.8 V vs. Ag/AgCl under light illumination conditions. It is found that both cubic and hexagonal ZIS exhibit similar photoelectrochemical water splitting properties under visible light illumination. This indicates the potential of ZIS as efficient photoelectrodes for sustainable hydrogen production through water splitting.

In order to improve PEC performance, coupling a visible light active conducting polymer polyaniline (PANI) using a simple chemisorption method is a good choice for the efficient charge transfer and good photo response of the material. Because of its hole-trapping and electron-donating nature, it helps in reducing charge carrier recombination in the nanocomposites. The PEC performance of the nanocomposite (C-ZIS/PANI) has been studied. The photocurrent density of the C-ZIS/PANI nanocomposite photoelectrode exhibits ~3-time enhancement (~260 $\mu A/cm^2$ at 0.8 V vs. Ag/AgCl) as compared to C-ZIS photoelectrode under

light illumination.

Further to improve PEC performance, hexagonal phase $ZnIn_2S_4$ (H-ZIS) has been synthesized using a hydrothermal method and coupled with visible light active g-C_3N_4 (C_3N_4) nanosheets using the chemisorption method. The current density in the case of H-ZIS/C_3N_4 photoanodes reaches ~110 μA/cm^2 at 0.8 V vs. Ag/AgCl, which is ~1.9 times higher than H-ZIS photoanode. The current density of the H-ZIS/C_3N_4 photoanode is increased due to the addition of C_3N_4 onto H-ZIS and the formation of a heterojunction between H-ZIS and C_3N_4, which supports a decrease in recombination due to efficient separation of photogenerated electron-hole pairs.

Finally, to enhance the PEC performance of H-ZIS photoelectrode, layered hexagonal zinc indium sulfide coupled multiwalled carbon nanotubes (MWCNTs/H-ZIS) nanocomposites were synthesized using hydrothermal method and its performance towards photoelectrochemical water splitting activity was studied. A series of MWCNTs/H-ZIS nanocomposites with different concentrations of MWCNTs has been synthesized. The effects of the composite ratio in the MWCNTs/H-ZIS on the photoelectrochemical performance were investigated. The highest photocurrent density in the case of 20 wt % MWCNTs/H-ZIS nanocomposite photoanodes reaches ~224 μA/cm^2 at 0.8 V vs. Ag/AgCl, which is ~3.8 times higher than H-ZIS photoanode. The enhancement in the current density is because of electron accepting behavior of MWCNT that helps in efficient separation of photogenerated electron-hole pair and faster transfer of charges across the interface. The electron-accepting and electron-transport capabilities of MWCNT offer an easy way to regulate the flow of photogenerated charge carriers, prolonging the lifetime of the photogenerated electron-hole pairs produced by semiconductors.

सारांश

औद्योगिक और शहरी क्रांतियों की शुरुआत के बाद से निरंतर बिजली की खपत अर्थव्यवस्था को चला रही है। हालाँकि, इस मांग को पूरा करने के लिए जीवाश्म ईंधन को जलाने से ग्लोबल वार्मिंग और कई स्वास्थ्य समस्याएं पैदा हुई हैं, जिससे सतत और पर्यावरण-अनुकूल ऊर्जा स्रोत की खोज भविष्य की पीढ़ियों के लिए एक गंभीर मुद्दा बन गई है। दहन-आधारित ऊर्जा रूपांतरण प्रक्रिया विशेष रूप से समस्या ग्रस्त है और इसके लिए कार्बन मुक्त और नवीकरणीय ऊर्जा स्रोत के विकास की आवश्यकता है जो पर्यावरण को नुकसान पहुंचाए बिना समाज को लाभ पहुंचा सके। हाइड्रोजन ईंधन एक आशाजनक विकल्प है जो इन आवश्यकताओं को पूरा कर सकता है। सतत ऊर्जा पैदा करने का एक महत्वपूर्ण तरीका फोटोइलेक्ट्रोकेमिकल (PEC) जल विभाजन है, जो हाइड्रोजन और आक्सीजन का उत्पादन कर सकता है। यह अध्ययन सेमीकंडक्टर नैनोस्ट्रक्चर और नैनोकम्पोजिट के संश्लेषण पर केंद्रित है और हाइड्रोजन उत्पन्न करने के लिए फोटोइलेक्ट्रोकेमिकल जल विभाजन के लिए इसके अनुप्रयोग का पता लगाता है।

इस दिशा में काम करने के लिए, दो अलग-अलग पूर्ववर्तियों का उपयोग करके हाइड्रोथर्मल विधि द्वारा दृश्य प्रकाश सक्रिय $ZnIn_2S_4$ (ZIS) के क्यूबिक और हेक्सागोनल फेज की सिंथेसिस की गई और इसके PEC जल विभाजन में उपयोग की संभावना का अन्वेषण किया गया। मटेरियल के फेज को नियंत्रित करने में पूर्ववर्तियों का चयन महत्वपूर्ण भूमिका निभाता है। विभिन्न विश्लेषण तकनीकों का उपयोग करके ZIS के संरचनात्मक, रूपात्मक और ऑप्टिकल गुणों का विश्लेषण किया गया। इसके अतिरिक्त, निर्मित ZIS फोटोइलेक्ट्रोड के PEC गुणों की जांच की गई। क्यूबिक-ZIS (C-ZIS) फोटोइलेक्ट्रोड ने 0.8 V vs. Ag/AgCl पर ~80 $\mu A/cm^2$ का प्रकाश धारा घनत्व हासिल किया, जबकि हेक्सागोनल ZIS (H-ZIS) ने 0.8 V vs. Ag/AgCl पर लगभग 60 $\mu A/cm^2$ का प्रकाश धारा घनत्व हासिल किया। यह पाया गया है कि C-ZIS और H-ZIS दोनों दृश्य प्रकाश की उपस्थिति मे समान PEC जल विभाजन गुण प्रदर्शित करते हैं। यह जल विभाजन के माध्यम से सतत हाइड्रोजन उत्पादन के लिए कुशल फोटोइलेक्ट्रोड के रूप में ZIS की क्षमता को इंगित करता है।

PEC प्रदर्शन में सुधार करने के लिए, एक सरल रसायन-अवशोषण विधि का उपयोग करके एक दृश्य प्रकाश सक्रिय संवाहक पॉलिमर पॉलीएनिलिन (PANI) को युग्मित करना कुशल चार्ज ट्रांसफर और सामग्री की अच्छी फोटो प्रतिक्रिया के लिए एक अच्छा विकल्प है। इसकी धनावेश वाहक (होल) फँसाने और ऋणावेश वाहक (इलेक्ट्रॉन) दान प्रकृति के कारण, यह नैनोकम्पोजिट में चार्ज वाहक पुनर्संयोजन को कम करने में मदद करता है। नैनोकम्पोजिट (C-ZIS/PANI) के PEC प्रदर्शन का अध्ययन किया गया है। C-ZIS/PANI नैनोकम्पोजिट फोटोइलेक्ट्रोड का प्रकाश धारा घनत्व C-ZIS फोटोइलेक्ट्रोड की तुलना में

~3 गुना वृद्धि (~260 μA/cm^2 at 0.8 V vs Ag/AgCl) प्रदर्शित करता है।

PEC प्रदर्शन को बेहतर बनाने के लिए, हेक्सागोनल चरण $ZnIn_2S_4$ (H-ZIS) को हाइड्रोथर्मल विधि का उपयोग करके संश्लेषित किया गया है और रसायन अवशोषण विधि का उपयोग करके दृश्य प्रकाश सक्रिय g-C_3N_4 (C_3N_4) नैनोशीट्स के साथ जोड़ा गया है। H-ZIS/C_3N_4 फोटोएनोड के मामले में प्रकाश धारा घनत्व 0.8 V vs. Ag/AgCl पर ~110 μA/cm^2 तक पहुंच जाता है, जो H-ZIS फोटोएनोड से ~1.9 गुना अधिक है। H-ZIS/C_3N_4 फोटोएनोड का प्रकाश धारा घनत्व, H-ZIS पर C_3N_4 के जुड़ने और H-ZIS और C_3N_4 के बीच एक हेटेरोजंक्शन के गठन के कारण बढ़ जाता है, जो फोटोजेनरेटेड इलेक्ट्रॉन के कुशल पृथक्करण के कारण पुनर्संयोजन में कमी का समर्थन करता है।

अंत में, H-ZIS फोटोइलेक्ट्रोड के PEC प्रदर्शन को बढ़ाने के लिए, H-ZIS युग्मित मल्टीवॉल्ड कार्बन नैनोट्यूब (MWCNTs/H-ZIS) नैनोकम्पोजिट को हाइड्रोथर्मल विधि का उपयोग करके संश्लेषित किया गया और PEC जल विभाजन गतिविधि के प्रति इसके प्रदर्शन का अध्ययन किया गया। MWCNTs की विभिन्न सांद्रता वाले MWCNTs/H-ZIS नैनोकम्पोजिट की एक श्रृंखला को संश्लेषित किया गया है। PEC प्रदर्शन पर MWCNTs/H-ZIS में मिश्रित अनुपात के प्रभावों की जांच की गई। 20 wt % MWCNTs/H-ZIS नैनोकम्पोजिट फोटोएनोड के मामले में उच्चतम प्रकाश धारा घनत्व 0.8 V vs. Ag/AgCl पर ~224 μA/cm^2 तक पहुंच जाता है, जो H-ZIS फोटोएनोड से ~3.8 गुना अधिक है। प्रकाश धारा घनत्व में वृद्धि MWCNT के इलेक्ट्रॉन स्वीकार करने वाले व्यवहार के कारण है जो फोटोजेनरेटेड इलेक्ट्रॉन-होल जोड़ी के कुशल पृथक्करण और इंटरफ़ेस में चार्ज के तेजी से हस्तांतरण में मदद करता है। MWCNT की इलेक्ट्रॉन-स्वीकृति और इलेक्ट्रॉन-परिवहन क्षमताएं फोटोजेनरेटेड चार्ज वाहक के प्रवाह को विनियमित करने का एक आसान तरीका प्रदान करती हैं, जो अर्धचालकों द्वारा उत्पादित फोटोजेनरेटेड इलेक्ट्रॉन-होल जोड़े के जीवनकाल को बढ़ाती है।

Table of Contents

Certificate **i**
Acknowledgements **ii-iii**
Abstract **iv-v**
Table of contents **vi-x**
List of figures **xi-xv**
List of tables **xvi**
Nomenclature **xvii-xviii**

CHAPTER 1: Introduction **1-30**
1.1 Overview 2
1.2 Photoelectrochemical (PEC) Water Splitting 4
1.2.1 Working Principle 4
1.2.2 Photoelectrochemical cell 6
1.2.3 Electrode/Electrolyte Interface 7
1.3 Photoelectrode Materials and their requirements 8
1.4 Challenges and Strategies 12
1.5 Different strategies to develop efficient photoelectrode material 13
1.5.1 Formation of heterojunction 13
1.5.1.1 Types of heterojunctions 13
1.5.2 Formation of different kind of nanocomposites system 15
1.6 Materials of interest 16
1.6.1 Zinc Indium Sulphate ($ZnIn_2S_4$) 17
1.6.2 g-C_3N_4 18
1.6.3 Multiwalled carbon nanotubes (MWCNTs) 19
1.7 Motivation of the Work 20
1.8 Objectives of the Thesis 21
1.9 Outline of the Thesis 22
References

CHAPTER 2: Experimental Details and Characterization Techniques **31-51**
2.1 Introduction 32
2.2 Synthesis method 32
2.2.1 Hydrothermal Method 32
2.2.2 Thermal polymerization method 34
2.2.3 Fabrication of Photoelectrode 34

2.3 Characterization Techniques 35
2.3.1 X-ray Diffraction 35
2.3.2 Field Emission Scanning Electron Microscopy 37
2.3.3 Energy Dispersive X-ray Spectroscopy 39
2.3.4 Transmission Electron Microscopy 40
2.3.5 UV-Visible Spectroscopy 41
2.3.6 Photoluminescence Spectroscopy 44
2.3.7 X-ray Photoelectron Spectroscopy 45
2.4 Photoelectrochemical Measurements 46
2.4.1 Linear Sweep Voltammetry (LSV) 47
2.4.2 Electrochemical Impedance Spectroscopy (EIS) 48
2.4.3 Mott-Schottky (M-S) 49
2.4.4 Incident Photon to Current Conversion Efficiency (IPCE) 49
References
CHAPTER 3: Synthesis of $ZnIn_2S_4$ for Photoelectrochemical Water Splitting 52-73
3.1 Introduction 53
3.2 Experimental Section 54
3.2.1 Synthesis of Cubic $ZnIn_2S_4$ 54
3.2.2 Synthesis of Hexagonal $ZnIn_2S_4$ 55
3.3 Results and Discussions 56
3.3.1 Structural Analysis 56
3.3.2 Morphological Analysis 57
3.3.3 Energy Dispersive X-ray Spectroscopy and Elemental Mapping Study 58
3.3.4 UV-Visible Absorption Spectroscopy Study 59
3.3.5 Photoelectrochemical Measurements 60
3.3.5.1 Linear Sweep Voltammetry Study 60
3.3.5.2 Electrochemical Impedance Spectroscopy Study 61
3.3.5.3 Mott-Schottky Study 62
3.4 Results and Discussion 63
3.4.1 Structural Analysis 63
3.4.2 Morphological Analysis 64
3.4.3 Energy Dispersive X-ray Spectroscopy and Elemental Mapping Study 65
3.4.4 UV-Visible Absorption Spectroscopy Study 66
3.4.5 Photoelectrochemical Measurements 66

3.4.5.1 Linear Sweep Voltammetry Study 67
3.4.5.2 Electrochemical Impedance Spectroscopy Study 67
3.4.5.3 Mott-Schottky Study 69
3.5 Photoelectrochemical Reaction Mechanism 69
3.6 Conclusion 71
References
CHAPTER 4: Enhanced Photoelectrochemical Water Splitting Performance of Visible Light Active $ZnIn_2S_4$/PANI Nanocomposite. **74-93**
4.1 Introduction 75
4.2 Experimental Section 76
4.2.1 Synthesis of Cubic $ZnIn_2S_4$ (C-ZIS) 76
4.2.2 Synthesis of C-ZIS/PANI Nanocomposite 76
4.2.3 Photoelectrochemical measurements 77
4.3 Results and Discussions 77
4.3.1 Structural Analysis 77
4.3.2 Morphological and Elemental Analysis 78
4.3.3 UV-Vis Absorption Spectroscopy 81
4.3.4 Photoluminescence (PL) Spectroscopy 81
4.3.5 Brunauer-Emmett-Teller Measurement 82
4.3.6 Photoelectrochemical Measurements 83
4.3.6.1 Linear Sweep Voltammetry Study 83
4.3.6.2 Photoelectrochemical Water Splitting Mechanism 85
4.3.6.3 Electrochemical Impedance Spectroscopy 86
4.3.6.4 Mott-Schottky Study 87
4.3.6.5 Chronoamperometric Study 89
4.3.6.6 Photostability Test 90
4.3.6.7 Incident Photon to Current Conversion Efficiency 90
4.4 Conclusion 92
References
CHAPTER 5: Visible Light Active $ZnIn_2S_4$/g-C_3N_4 Heterostructure Nanocomposite Photoelectrode for Efficient Photoelectrochemical Water Splitting Activity. **94-112**
5.1 Introduction 95
5.2 Experimental Section 96
5.2.1 Synthesis of Hexagonal $ZnIn_2S_4$ (H-ZIS) 96

5.2.2 Synthesis of g-C_3N_4 96
5.2.3 Synthesis of H-ZIS/C_3N_4 Nanocomposite 96
5.2.4 Photoelectrochemical measurements 97
5.3 Results and Discussions 97
5.3.1 Structural Analysis 97
5.3.2 Morphological and Elemental Analysis 98
5.3.3 UV-Visible Absorption Spectroscopy 101
5.3.4 X-ray Photoelectron Spectroscopy 102
5.4 Photoelectrochemical Measurements 104
5.4.1 Linear Sweep Voltammetry Study 104
5.4.2 Photoelectrochemical Reaction Mechanism 105
5.4.3 Electrochemical Impedance Spectroscopy 107
5.4.4 Mott-Schottky Measurement 108
5.4.5 Incident Photon to Current Conversion Efficiency 109
5.5 Conclusions 111
References
CHAPTER 6: Enhanced photoelectrochemical water splitting in ternary layered chalcogenide $ZnIn_2S_4$ coupled with MWCNTs **113-129**
6.1 Introduction 114
6.2 Experimental Section 115
6.2.1 Synthesis of H-ZIS and MWCNTs/H-ZIS Nanocomposite 115
6.2.2 Photoelectrochemical measurements 116
6.3 Results and Discussions 116
6.3.1 Structural Analysis 116
6.3.2 Morphological and elemental Study 117
6.3.3 UV-Visible Absorption Spectroscopy 120
6.4 Photoelectrochemical Measurements 121
6.4.1 Linear Sweep Voltammetry Measurement 121
6.4.2 Photoelectrochemical Reaction Mechanism 122
6.4.3 Electrochemical Impedance Spectroscopy 123
6.4.4 Mott-Schottky Measurement 124
6.4.5 Incident Photon to Current Conversion Efficiency 126
6.5 Conclusion 127
References

CHAPTER 7: Conclusions and Future Scope **130-136**

7.1 Conclusions of the Present Study 130

7.2 Future Scope of Thesis 134

List of Publications 137

Poster/Oral presentations in National/International Conferences 138

Author Biodata 139

List of Figures

Figure 1.1 Schematic shows the fundamental steps involved in a PEC process.

Figure 1.2 Working principle for n-type and p-type semiconductors in a PEC process.

Figure 1.3 Schematic representation of a three electrode PEC cell assembly.

Figure 1.4 Different semiconducting materials suitable for oxidation, reduction and overall water splitting depending on their band edge position with respect to redox potential of water.

Figure 1.5 Showing different kinds of heterojunction (a) Type-I, (b) Type-II, and (c) Type-III heterojunction.

Figure 1.6 Showing crystal structure of $ZnIn_2S_4$: hexagonal phase, and cubic phase.

Figure 1.7 Schematic of different types of CNT (a) Single walled, (b) Double walled, and (c) Multi walled carbon nanotubes.

Figure 2.1 Experimental setup for hydrothermal synthesis of the $ZnIn_2S_4$.

Figure 2.2 (a) Schematic diagram and (b) image of fabricated photoelectrode used for PEC measurements, respectively.

Figure 2.3 Schematic diagram of basic principle of X-ray diffraction.

Figure 2.4 Image of X-ray diffraction (XRD) instrument (Rigaku Ultima IV) used for phase analysis.

Figure 2.5 Schematic of FESEM and actual image of FESEM instrument used for morphological analysis.

Figure 2.6 Image of EDS instrument used for elemental analysis and mapping of $ZnIn_2S_4$.

Figure 2.7 (a) Basic layout of the component of TEM, (b) image of TEM instrument used for TEM and HRTEM measurements.

Figure 2.8 Schematic diagram of UV-vis spectrophotometer used to analyze the optical properties.

Figure 2.9 Image of UV-vis instrument used in this thesis for optical absorption analysis.

Figure 2.10 Image of actual instrument used in this work to analyze the photoluminescence (PL) properties.

Figure. 2.11 Schematic of the steps involved in performing x-ray photoelectron

spectroscopy (XPS) measurements.
Figure 2.12 Image of XPS instrument used to analyze the chemical states of material
Figure 2.13 Experimental setup for performing photoelectrochemical (PEC) measurements.
Figure 3.1 Schematic of the steps involved in the synthesis of C-ZIS.
Figure 3.2 Schematic of the steps involved in the synthesis of H-ZIS.
Figure 3.3 XRD spectra of the as synthesized C-ZIS sample.
Figure 3.4 (a) FESEM image of C-ZIS, and (b) TEM image C-ZIS sample.
Figure 3.5 (a) Selected area for EDX analysis, (b) EDX spectra corresponding to selected area of C-ZIS sample, and the respective elemental mapping image of (c) Zn (red), (d) In (green), (e) S (blue), and (f) color overlay of Zn, In and S elements distribution.
Figure 3.6 UV-vis absorption spectra and the corresponding tauc's plot (inset image) of C-ZIS.
Figure 3.7 Linear sweep voltammetry (LSV) curve of C-ZIS nanoflakes photoelectrode.
Figure 3.8 Nyquist plots of C-ZIS under dark and light illumination condition.
Figure 3.9 Mott-Schottky (M-S) plot for C-ZIS photoelectrode.
Figure 3.10 XRD spectra of as-synthesized H-ZIS.
Figure 3.11 (a) FESEM image, and (b) TEM image of H-ZIS, respectively.
Figure 3.12 (a) Selected area for EDX analysis, (b) EDX spectra corresponding to selected area of H-ZIS sample, and the respective elemental mapping image of (c) Zn (red), (d) In (green), (e) S (blue), and (f) color overlay of Zn, In and S elements distribution.
Figure 3.13 UV-vis spectra of H-ZIS and the inset shows the corresponding tauc's plot.
Figure 3.14 Linear sweep voltammetry (LSV) curve of H-ZIS photoelectrode.
Figure 3.15 Nyquist plots of H-ZIS under dark and light illumination condition.
Figure 3.16 Mott-Schottky (M-S) plot for H-ZIS photoelectrode.
Figure 3.17 Schematic diagram represents the charge transport phenomena in ZIS photoelectrode under light illumination condition.
Figure 4.1 Schematic for synthesis procedure of C-ZIS/PANI nanocomposite.
Figure 4.2 XRD pattern of PANI, C-ZIS and C-ZIS/PANI nanocomposite samples.
Figure 4.3 FESEM image of (a) C-ZIS, (b) C-ZIS/PANI nanocomposite. (c,d) shows

TEM images C-ZIS and C-ZIS/PANI nanocomposite, respectively.

Figure 4.4 **(a) Selected area SEM image for EDX analysis, (b) EDX spectra of C-ZIS/PANI nanocomposite, (c-g) Elemental mapping of C-ZIS/PANI nanocomposite, and (h) overlay image of Zn, In, and S.**

Figure 4.5 **UV-vis absorption spectra and their corresponding tauc's plots (inset image).**

Figure 4.6 **PL spectrum of C-ZIS and C-ZIS/PANI nanocomposites, respectively.**

Figure 4.7 **N_2 adsorption-desorption isotherm of (a) C-ZIS and (b) C-ZIS/PANI photoelectrode, respectively.**

Figure 4.8 **Linear sweep voltammetry (LSV) measurements for C-ZIS and C-ZIS/PANI nanocomposite photoelectrodes.**

Figure 4.9 **Schematic diagram represents the charge transport phenomena in C-ZIS/PANI nanocomposite photoelectrode under light illumination condition.**

Figure 4.10 **Nyquist plots of C-ZIS and C-ZIS/PANI nanocomposite photoelectrodes, respectively.**

Figure 4.11 **M-S curves for C-ZIS and C-ZIS/PANI nanocomposite photoelectrodes.**

Figure 4.12 **Chronoamperometric current–time (I–T) curves of C-ZIS and C-ZIS/PANI photoanode with 10 s ON/OFF cycle.**

Figure 4.13 **Photostability (I-t) test of C-ZIS and C-ZIS/PANI photoelectrodes, (b) XRD spectra of C-ZIS/PANI nanocomposite photoelectrode before and after performing PEC measurements.**

Figure 4.14 **IPCE spectra of the C-ZIS and C-ZIS/PANI nanocomposite photoelectrode at bias of 0.8 V.**

Figure 5.1 **Schematic of different steps for the synthesis of (a) g-C_3N_4, and (b) H-ZIS/C_3N_4 nanocomposite.**

Figure 5.2 **XRD spectra of g-C_3N_4, H-ZIS and H-ZIS/C_3N_4 nanocomposite.**

Figure 5.3 **FESEM image of (a) H-ZIS, (b) H-ZIS/C_3N_4 nanocomposite, TEM images of (c) H-ZIS, (d) H-ZIS/C_3N_4, HRTEM images of (e) H-ZIS and (f) H-ZIS/C_3N_4 nanocomposite respectively.**

Figure 5.4 **(a) Selected area of SEM image for EDX analysis, (b) EDX spectra of H-ZIS/C_3N_4 nanocomposite, (c-g) Elemental mapping of H-ZIS/C_3N_4 nanocomposite, and (h) overlay image of Zn (red), In (green), and S (blue).**

Figure 5.5 **UV-vis spectra of H-ZIS and H-ZIS/C_3N_4 nanocomposite and the inset**

shows the corresponding tauc's plot.

Figure 5.6 **XPS spectra of H-ZIS and H-ZIS/C_3N_4 nanocomposite. (a) survey spectrum of H-ZIS/C_3N_4, (b) Zn 2p, (c) In 3d, (d) S 2p, (e) C 1s, and (f) N 1s core level spectra.**

Figure 5.7 **Current vs. voltage curve for H-ZIS and H-ZIS/C_3N_4 nanocomposite under dark and light illumination.**

Figure 5.8 **Schematic diagram of PEC water splitting over the H-ZIS/C_3N_4 nanocomposite photoanode.**

Figure 5.9 **EIS spectra for H-ZIS and H-ZIS/C_3N_4 nanocomposite under light illumination.**

Figure 5.10 **Mott-Schottky plots of H-ZIS and H-ZIS/C_3N_4 nanocomposite photoanodes.**

Figure 5.11 **IPCE spectra of H-ZIS and H-ZIS/C_3N_4 nanocomposite photoanode at 0.8 V.**

Figure 6.1 **Schematic representation for the synthesis of MWCNT/H-ZIS nanocomposite.**

Figure 6.2 **XRD patterns of MWCNT, H-ZIS, and MWCNT/H-ZIS nanocomposites samples with varying concentration of MWCNTs (a =10, b = 15, c = 20, and d = 25 wt %).**

Figure 6.3 **FESEM image of H-ZIS and 20 MWCNT/H-ZIS nanocomposite.**

Figure 6.4 **(a) Selected area of SEM image for EDX analysis, (b) EDX spectra, and (c-g) corresponding elemental mapping image of MWCNT/H-ZIS nanocomposite.**

Figure 6.5 **Tauc's plot for estimating the bandgap of H-ZIS and MWCNT/H-ZIS nanocomposite.**

Figure 6.6 **(a) LSV curve for H-ZIS and 20 wt % of MWCNT in MWCNT/H-ZIS nanocomposite under dark and light illumination and (b) shows the current density (under light illumination at 0.8 V) of MWCNT/H-ZIS photoanode with different wt % of MWCNT (10, 15, 20, and 25 wt %).**

Figure 6.7 **(a) Schematic representation showing fermi level of MWCNT and CB and VB edge position of H-ZIS and (b) charge transfer mechanism for PEC water splitting reaction over the MWCNT/H-ZIS nanocomposite photoanode.**

Figure 6.8 **(a) EIS Nyquist plot of H-ZIS and 20 wt % MWCNT/H-ZIS**

nanocomposite photoanodes under the light illumination condition and (b) charge transfer resistance (R_{ct}) with different wt % of MWCNT in the nanocomposites.

Figure 6.9 **M-S analysis of H-ZIS and MWCNT/H-ZIS nanocomposite photoanode.**

Figure 6.10 **IPCE plot of H-ZIS and MWCNT/H-ZIS nanocomposite photoanode.**

List of Tables

Table 4.1 **Comparison of surface area and pore volume of C-ZIS and C-ZIS/PANI samples.**

Table 4.2 **Comparison of the photocurrent density of C-ZIS/PANI with the earlier reported results for water splitting.**

Table 4.3 **List of corresponding data of equivalent circuit obtained from EIS measurement.**

Table 5.1 **Comparison of the photocurrent density of H-ZIS/C_3N_4 with other C_3N_4 based nanocomposites published work for PEC application.**

Nomenclature

Symbols

e	Electronic charge
ε_0	Permittivity of vacuum
ε_r	Dielectric constant
N_d	Donor density
V	Applied potential
V_{fb}	Flat band potential
K_B	Boltzmann constant
T	Absolute temperature
θ	Phase angle
Z'	Real part of the impedance
Z''	Imaginary part of the impedance
R_s	Solution resistance
R_{ct}	Charge transfer resistance
C_{dl}	Double layer capacitance
J_p	Photocurrent density
λ	Wavelength of the incident monochromatic light
P	Incident power density

Abbreviations

CB	Conduction band
CCD	Charged coupled device
DI	Deionized
EDS	Energy dispersive X-ray spectroscopy
EIS	Electrochemical impedance spectroscopy
FTO	Fluorine doped tin oxide
HRTEM	High resolution transmission electron microscopy
IPCE	Incident photon to current conversion efficiency
JCPDS	Joint committee on powder diffraction standards
LSV	Linear sweep voltammetry
NHE	Normal hydrogen electrode
MS	Mott-Schottky
OER	Oxygen evolution reactions
PEC	Photoelectrochemical
PL	Photoluminescence spectroscopy
SEM	Scanning electron microscopy
TEM	Transmission electron microscopy
THF	Tetrahydrofuran
UV	Ultraviolet
UV-vis	UV-vis spectroscopy
VB	Valence band
XRD	X-ray diffraction